York University

GNSS Data Collection, Processing, and Analysis

Project 2: Final Report

Agata Szeremeta - 213 400 148
C olin Vanderwoerd - 214 815 328
Dawid Szeremeta - 213 957 030
Mitch Palmer - 213 475 769

ESSE 4610: Global Positioning Systems
Dr. Sunil Bisnath
February 12, 2018

Table of Contents

Executive Summary

The purpose of this report is to explore the factors that influence GNSS positional accuracy. Utilizing both an in-field method and a research approach, factors contributing to accuracy degradation will be discussed.

The first approach was to conduct field observations to investigate environmental effects on signal quality. Using the location of a known point as a base station, differential GNSS positioning was applied to acquire the location of three surrounding points. One point was underneath a canopy of tree branches, another was adjacent to a wall of a building, and the final point was in an open field. GNSS observations were collected 3 times for each point at different times.

The second approach was to inspect data from two base-stations available through the SOPAC database. Data over a 7 day period was collected and analyzed to reveal accuracy parameters. In particular, the receiver's signal frequency and elevation cutoff was altered to produce various observation scenarios.

Utilizing *Leica Infinity* software we were able to process the information to reveal coordinates in the WGS84 and NAD83 CSRS UTM Zone 17 coordinate systems. In order to infer the effects on positional accuracy, the following parameters were studied:

- 1D, 2D and 3D measurement rms errors ("CQs")
- GDOP, PDOP, HDOP and VDOP
- The number of satellites tracked vs. the number of satellites available

From the results we see multipath error as a large contributor of positional accuracy degradation. In addition to this, the duration of time, signals received and the geometry of the satellites observed, all play a role in the accuracy of the acquired position.

Introduction

GNSS antennas, along with paired receivers, can be utilized to precisely locate a position on Earth. This position is based on a variety of predictable factors, the largest of which has to do with the number of visible satellites. Increasing the number of satellites observed at a particular time results in an overdetermined system (minimum of 4 satellites required to have a unique solution). By applying least squares we can utilize redundant observations to compute the best estimate of the antenna's position. Thus, two different approaches can be used to gain better accuracy through GNSS positioning:

1. One could increase the duration of time spent observing the satellites. With increased observations, our system becomes more redundant allowing better estimation. In addition to this, through time, the satellite geometry alters, providing variation in the satellite distribution geometry.
2. Ensure the antenna is not obstructed. Fewer obstructions provides a clearer path of travel for satellite signals (limits multipath error), and allows signal visibility between an antenna and other satellites.

Unfortunately, even with these procedures, precise GNSS antennas have limited accuracies. Fortunately, by utilizing the differential GNSS method, we are capable of achieving centimeter level accuracy. The differential GNSS method utilizes one GNSS antenna as a base station (over a known point), and one antenna as a mobile receiver. By looking at the differences observed by these two antennas, we are capable of acquiring a greater accuracy for the mobile GNSS antenna.

To simplify the procedures, there exists a network of base-stations operated by organizations such as SOPAC, IGS, Cansel's CANNET, and Leica's SMARTNET, located across Canada. These organizations provide continuous updates on the GNSS data collected by their base-stations as a service for differential GNSS processing.

Using the differential GNSS method, this report inspects how various factors are capable of diluting the precision of GNSS positioning. In particular, this report will inspect how antenna obstructions, satellite geometry, types of signals received and satellite elevations influence the accuracy of GNSS positioning. Through the implementation of an in-field and research approach, it is expected that these factors greatly influence the success of the observations.

Methods

Part 1: Static Data Collection and Processing

Field Procedures

To begin the in-field approach, a high precision GNSS antenna and receiver was set up over a known point. This point was to be used as our reference station during data processing. Its location can be roughly seen in the following diagram.

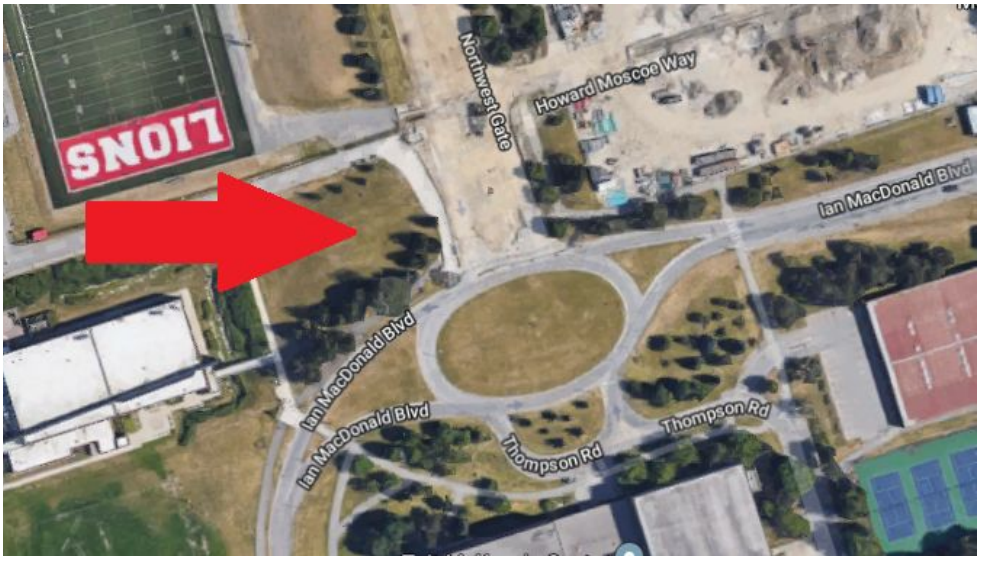

Figure 1: Location of Known Station to be Set as Reference Station

Using a tribrach and tripod, the antenna was positioned and leveled precisely over the point. The GNSS receiver was then paired with the antenna, and set to limit observations to the GPS constellation. With the parameters set, the receiver was set to record observations until the end of the experiment.

With the base station set, three points were marked out near the base-station. The first station was set under a tree canopy, the second station was set in an open field, while the last station was set adjacent to a wall of a two storey structure (Western wall of Tait Mckenzie building). These points were temporarily marked for the subsequent observations. The location of these points can be seen in the following diagrams (indicated by circles in the campus map).

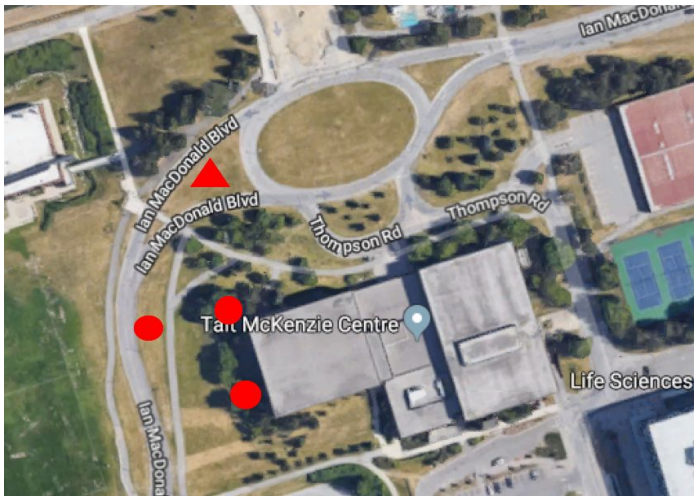

Figure 2: Station Underneath Tree Canopy

Figure 3: Station in an Open Field

Figure 4: Station Adjacent to a Wall

Using a second GNSS antenna and receiver, static measurements were taken at each of the three points according to the following procedure:

- The antenna was set-up and leveled over the point using a tripod and tribrach. The antenna height was ignored, as it was irrelevant for our purposes.
- Once a fix was obtained, data was collected for at least two minutes.
- The antenna was then set up on the subsequent point.
- The three points were cycled such that adequate time lapsed before the same point was measured again. This ensured a large enough variation in satellite geometry, as roughly 7 minutes passed before each point was measured again.

Using this protocol, a total of 9 measurements were taken (3 at each point). Upon completion, the observation at the base antenna was terminated and stored.

Office Procedures

Once all observations were conducted, the project file was downloaded from the data collector and processed through *Leica Infinity* software.

To process the data, a new project was created in Leica Infinity, with the display coordinate system set to both the local system and WGS84. With the project setup, we imported the data collected in the field through the *Import* tool. With the observations imported, we set the base station to be the static reference station, while all other observations were set to mobile rover stations. The parameters set, the duration of each observation, along with other properties can be observed in the following diagram.

	Point Id	Start Time	End Time	Duration	Sampling Rate...	Height Reading [m]	Antenna Height [m]			Receiver SN
	BASESTATION	01/29/2018 14:37:34	01/29/2018 16:02:43	01:25:09	1.00	1.5500	1.5500	...	...	2912188
	open1	01/29/2018 14:57:56	01/29/2018 15:01:26	00:03:30	5.00	1.5920	1.5920	...	...	2912152
	tree1	01/29/2018 15:04:47	01/29/2018 15:08:13	00:03:26	5.00	1.5920	1.5920	...	...	2912152
	building1	01/29/2018 15:13:33	01/29/2018 15:18:02	00:04:29	5.00	1.5920	1.5920	...	...	2912152
	open2	01/29/2018 15:21:49	01/29/2018 15:24:57	00:03:08	5.00	1.5920	1.5920	...	...	2912152
	tree2	01/29/2018 15:27:49	01/29/2018 15:30:54	00:03:05	5.00	1.5920	1.5920	...	...	2912152
	building2	01/29/2018 15:34:26	01/29/2018 15:36:51	00:02:25	5.00	1.5920	1.5920	...	...	2912152
	open3	01/29/2018 15:42:19	01/29/2018 15:45:15	00:02:56	5.00	1.5920	1.5920	...	...	2912152
	tree3	01/29/2018 15:49:42	01/29/2018 15:52:47	00:03:05	5.00	1.5920	1.5920	...	...	2912152
	building3	01/29/2018 15:56:26	01/29/2018 15:59:04	00:02:38	5.00	1.5920	1.5920	...	...	2912152

Figure 5: Observation Properties

A clear depiction of the sequence of observations and their durations can be seen in the following diagram.

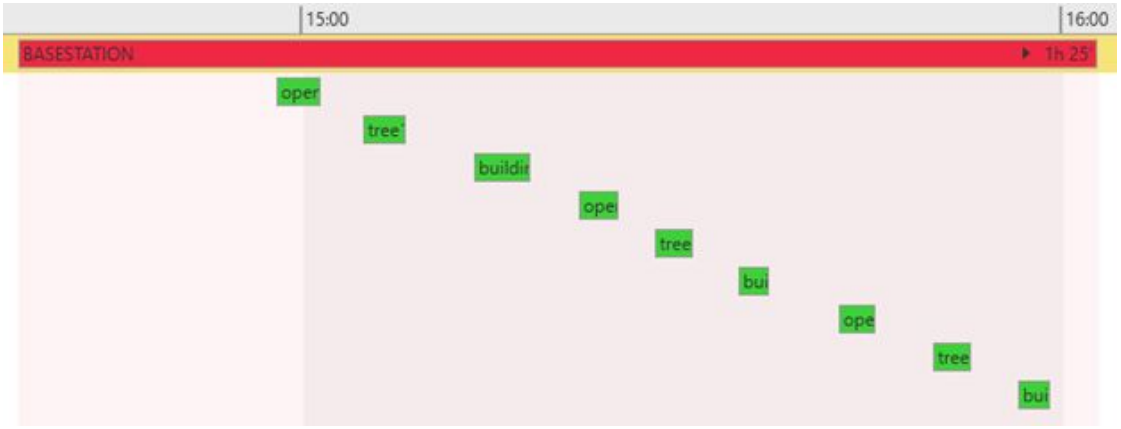

Figure 6: Time Stamps for Observations

With the parameters set, we used the process tool to compute the baselines, coordinates and standard deviations. With the observations processed it is possible to view the baseline observations in the local coordinate system (NAD83 UTM 17N CSRS). We can visually inspect our observations and computed baselines by viewing the output against a base map (Figure: 7). This diagram agrees with the infield positions of our stations. As such, our post-field processing is validated.

Figure 7: Stations and Baselines Observed

The post processing coordinates, along with the baseline components and their standard deviations can be seen in the results section.

Using the standard deviation for the baseline components, we computed the 3D standard deviation utilizing the following expression.

$$\sigma_{3D} = \sqrt{\sigma_x^2 + \sigma_y^2 + \sigma_z^2}$$

The results for our computations will be analyzed to determine how our GNSS observations were affected by the various station positions.

Part 2: Static data Processing and Analysis

Data Downloading

Data from November 25, 2017 to December 1, 2017 was downloaded from the SOPAC data browser. Using the Data by Date search tool, data of types Products and Observations from GPS Week 1976 (corresponding to the last week of November 2017 and first week of December 2017) was found.

Downloading observation data from the ALBH GNSS service site was suggested. We were asked to download additional observation data from a site within 200km of ALBH. To find nearby sites, the International GNSS Service (or IGS) network was studied. This network was found through:

http://www.igs.org/network

The ALBH GNSS service site was located on the map. It was found that the site was within the city of Victoria of British Columbia in Canada and had latitude and longitude coordinates of 48.3898000 and -123.4874000. The site used a TPS NET-G3A receiver at a height of 32m. The site can be seen in the lower right corner of the figure below.

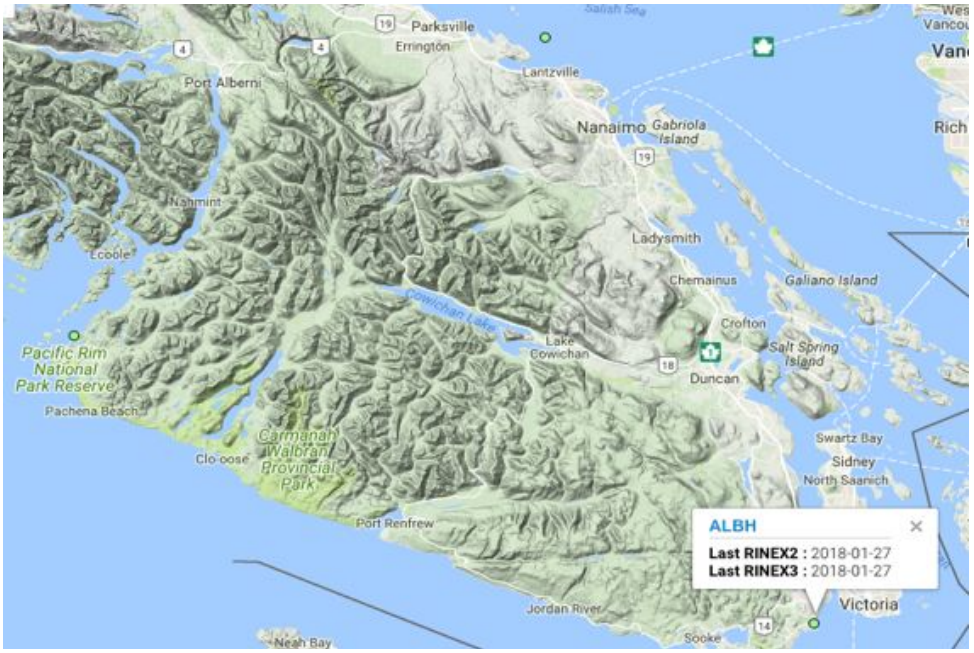

Figure 8: Location of ALBH GNSS Service Site

Studying the map, we observed the closest nearby stations to *ALBH* to be stations named *NANO* and *BAMF*.

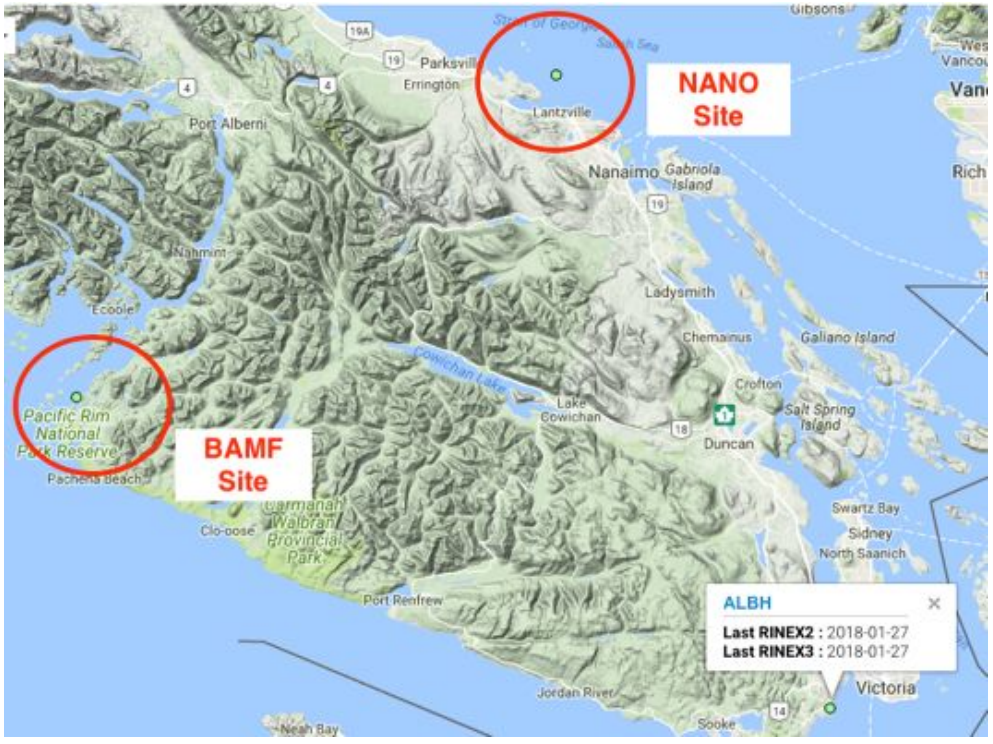

Figure 9: Location of Stations Near ALBH GNSS Service Site

To determine the distance between these sites and the *ALBH* site, they were plotted into Google Maps, using the provided approximate coordinates.

Table 1: Station Coordinates

GNSS Site	Site Coordinates	
	Latitude (◦)	Longitude (◦)
ALBH	48.3898000	-123.4874000
BAMF	48.8353167	-125.1350889
NANO	49.2948000	-124.0865000

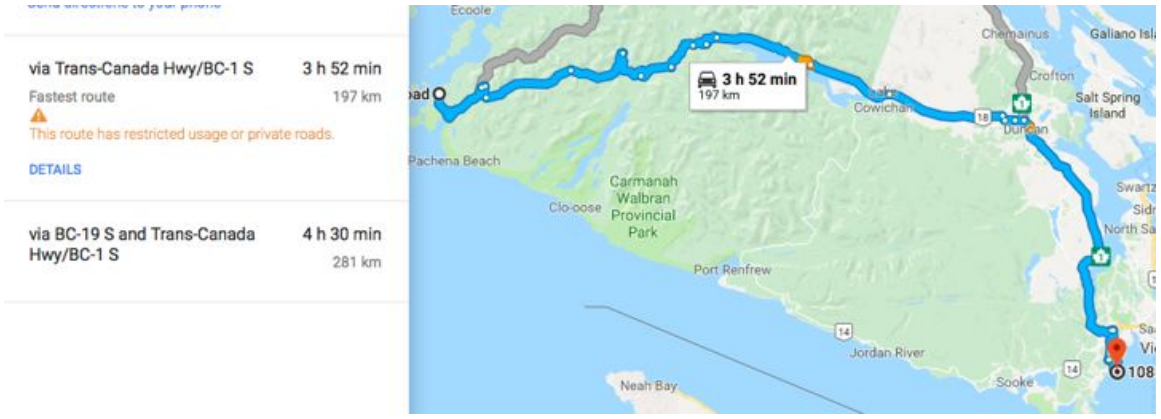

Figure 10: Distance from ALBH to BAMF Site

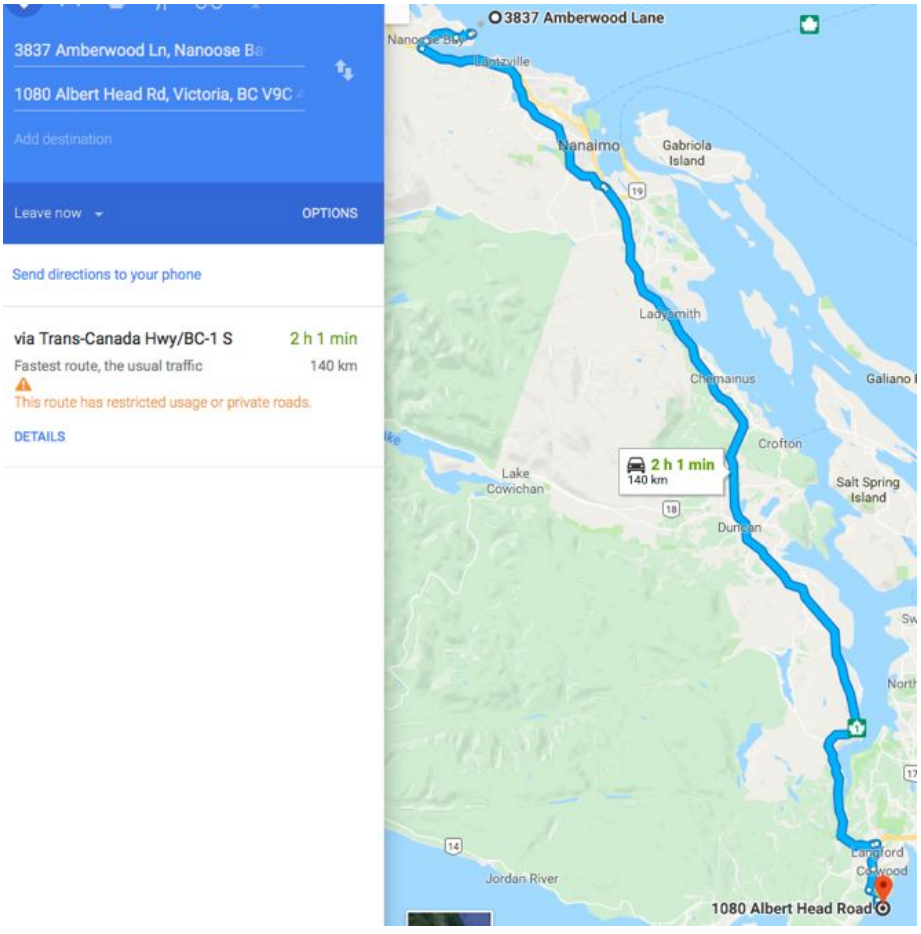

Figure 11: Distance from ALBH to NANO Site

The distance between the *ALBH* and *BAMF* sites was less than 197 km, while the distance between the *ALBH* and *NANO* sites was less than 140 km. Despite both being within range, the *BAMF* site was selected for study.

The following *Observation* data was downloaded from SOPAC for November 25 - December 1, 2017.

Table 2: Downloaded Observation Data

Day	***Observation* Name**	
	ALBH Site	***BAMF Site***
November 25	*albh3290.17d*	*bamf3290.17d*
November 26	*albh3300.17d*	*bamf3300.17d*
November 27	*albh3310.17d*	*bamf3310.17d*
November 28	*albh3320.17d*	*bamf3320.17d*
November 29	*albh3330.17d*	*bamf3330.17d*
November 30	*albh3340.17d*	*bamf3340.17d*
December 1	*albh3500.17d*	*bamf3500.17d*

Because it was noticed that the first day of downloaded observation data began on November 24 and not exactly November 25, it was necessary to download additional *igs* data to account for the ephemeris on that day. Thus, the following *Product* data was downloaded:

Table 3: Downloaded Product Data

Day of Week	***Product* Name**
1	igs19766.sp3
2	igs19770.sp3
3	igs19771.sp3
4	igs19772.sp3
5	igs19773.sp3
6	igs19774.sp3
7	igs19775.sp3
8	igs19776.sp3

The Standard Product #3 (or SP3, for short) is a NGS orbital format for Global Positioning System satellites. Unlike its predecessors, satellite clock correction information is sent in the SP3 format. These downloaded files provide ephemeris data regarding satellites.

Data Processing in Leica Infinity

All of the above downloaded data was imported into *Leica Infinity* software and a new project was created.

Upon creation of the new project, it was first necessary to define the local coordinate system in which the two sites fell in. From above, we observed both regions to be located on the south region of Vancouver Island, British Columbia. Using the website:

http://www.empr.gov.bc.ca/MINING/GEOSCIENCE/MAPPLACE/MAINMAPS/Pages/BCUTMZones.aspx

We identified the UTM Zones of British Columbia to be:

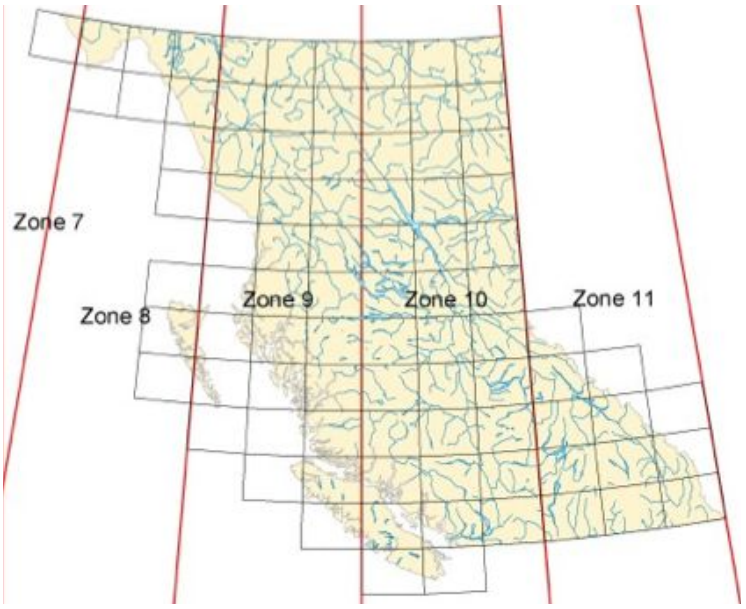

Figure 12: UTM Zones of British Columbia (British Columbia, n.d.)

We concluded that the *ALBH* and *BAMF* stations fall within Zone 10 of the UTM coordinate system. Using the *Localisation* tool, located under *File>Tools>Coordinate Systems* in the software, the BC UTM10 N83 local coordinate system was downloaded and applied to the project. This system made use of the GRS 1980 ellipsoid.

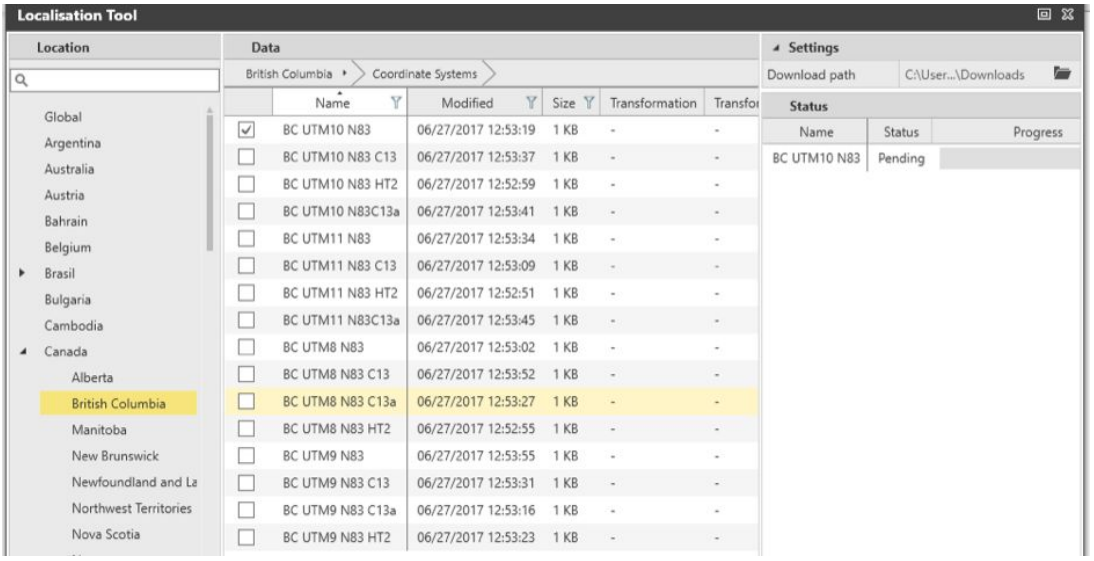

Figure 13: Setting Local Coordinate System

To ensure that the coordinate system was applied accordingly, we referred to the bottom right coordinate settings in the Leica Infinity View Window.

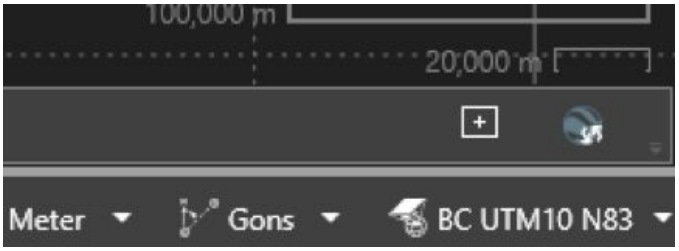

Figure 14: Ensuring Correct Application of Local Coordinate System

The GNSS data was ready for processing. Each of the 7 baselines were to be processed under the following conditions:

Table 4: Scenarios of Data Processing

Scenario	Data Arc (Hours)	Frequencies	Elevation Cutoff (◦)
1	**24**	**L1 and L2**	**10**
2	12	L1 and L2	10
3	1	L1 and L2	10
4	**24**	**L1**	**10**
5	12	L1	10
6	1	L1	10
7	**24**	**L1 and L2**	**15**
8	**24**	**L1 and L2**	**20**
9	**24**	**L1 and L2**	**25**

Due to the difficulties in altering the data arc in the software, only the scenarios with a 24 hour data arc were considered. That is, only scenarios 1, 4, 7, 8 and 9 were considered.

To begin processing, it was first necessary to identify the Reference (or "Base") and Rover stations in each station combination. For the purpose of this project, the *ALBH* sites were consistently selected as "base" or reference stations, while *BAMF* stations were selected as rover stations. Observations on the same date where chosen for study. These stations titles were set by simply right clicking on the station of interest under the *Inspector>GNSS* tab. The reference stations were highlighted in red, while the rover station where in green. An example of the result of this is shown below.

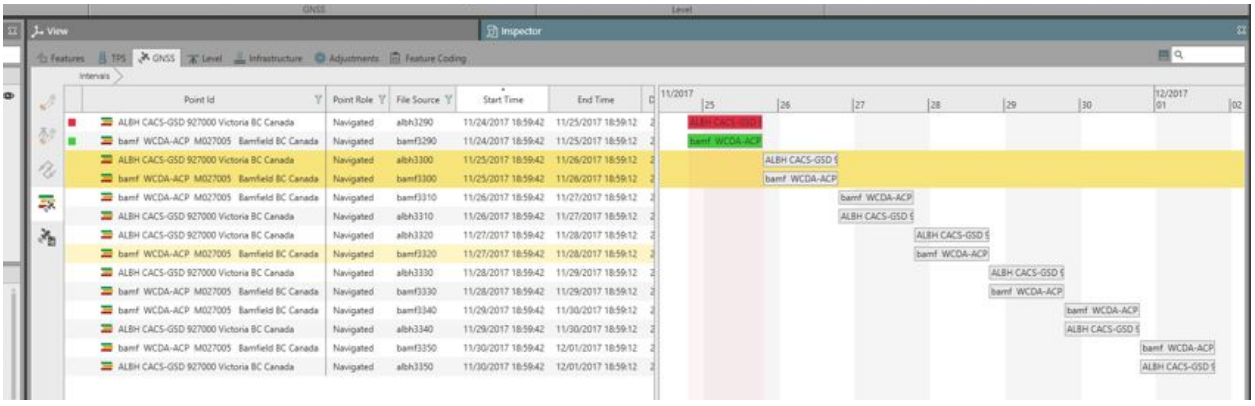

Figure 15: Example of Reference and Rover Stations

After selecting these stations, they could be observed under the *View* tab.

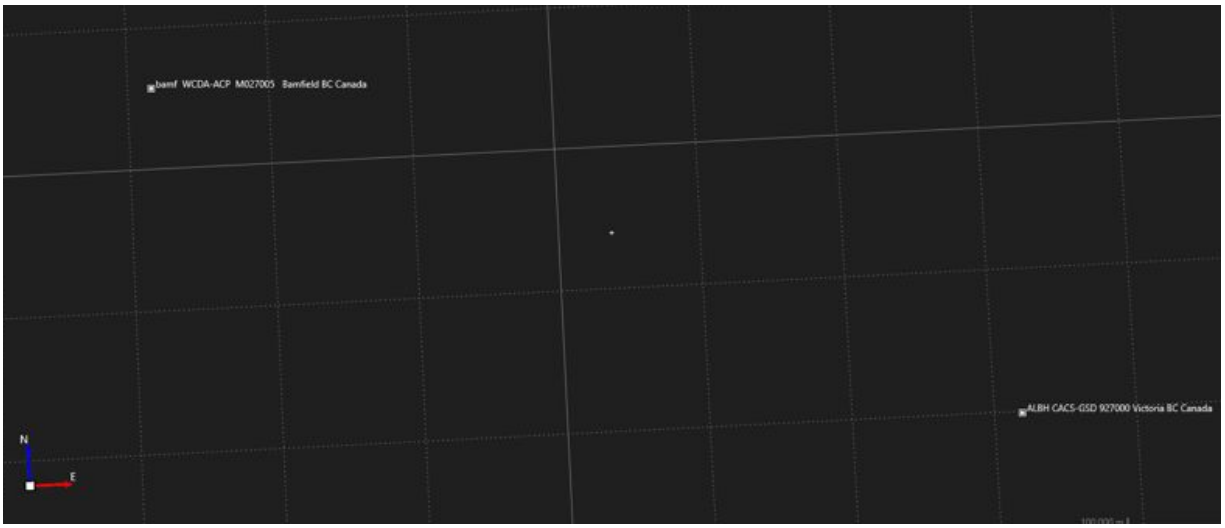

Figure 16: Plotted Stations

To modify the parameters to correspond to the various test scenarios in *Table 4* above, the processing settings were modified under the *Processing* tab. In particular, the cut-off frequency was modified under the *Data* tab while the frequencies under the *Advanced Settings* tabs. After processing, each scenario was saved as a CSV file. The estimate locations of the *BAMF* station and the standard deviations of the observed baselines were given.

Results

Part 1: Static Data Collection and Processing

The following are the results following processing of the field observations.

Table 5: Station Coordinates

Station	Obs. #	NAD83 UTM Zone 17		WGS84 Cartesian		
		Easting(m)	Northing (m)	X (m)	Y (m)	Z (m)
Open Field	**1**	619,830.863	4,847,913.760	839,772.907	-4,535,869.150	4,390,148.363
	2	619,830.858	4,847,913.767	839,772.907	-4,535,869.171	4,390,148.393
	3	619,830.862	4,847,913.765	839,772.916	-4,535,869.201	4,390,148.420
Tree	**1**	619,857.867	4,847,921.661	839,798.799	-4,535,859.866	4,390,154.404
	2	619,857.968	4,847,922.143	839,798.882	-4,535,859.714	4,390,154.941
	3	619,857.884	4,847,921.659	839,798.823	-4,535,859.908	4,390,154.445
Near Building	**1**	619,879.390	4,847,894.150	839,823.211	-4,535,876.206	4,390,135.416
	2	619,880.041	4,847,895.076	839,823.610	-4,535,874.688	4,390,135.321
	3	619,879.469	4,847,893.952	839,823.269	-4,535,876.104	4,390,135.054
Base Station	**1**	619,854.348	4,848036.199	839,783.520	-4,535,785.357	4,390,240.270

Table 6: Baselines Between Base Station and Station Point

Station	Obs. #	Baseline Components			Slope Distance (m)	Standard Deviation			
		ΔX (m)	ΔY (m)	ΔZ (m)		X (m)	Y (m)	Z (m)	3D (m)
Open Field	**1**	-10.612	-83.793	-91.907	124.823	0.0002	0.0005	0.0006	0.0008
	2	-10.613	-83.814	-91.877	124.815	0.0002	0.0005	0.0006	0.0008
	3	-10.604	-83.844	-91.850	124.815	0.0003	0.0006	0.0006	0.0009

Tree	**1**	15.279	-74.509	-85.867	114.709	0.0011	0.0030	0.0033	0.0046
	2	15.362	-74.357	-85.330	114.219	0.0395	0.0867	0.0950	0.1345
	3	15.304	-74.551	-85.825	114.709	0.0009	0.0018	0.0018	0.0027
Near Building	**1**	39.691	-90.849	-104.855	144.303	0.0014	0.0034	0.0029	0.0047
	2	40.090	-89.331	-104.949	143.532	0.0869	0.2101	0.1680	0.2827
	3	39.749	-90.747	-105.216	144.518	0.0469	0.0899	0.0696	0.1230

Table 7: GPS CQ values, DOP and GPS SVs

Station	**Obs. #**	**CQ 3D (m)**	**CQ 2D (m)**	**CQ 1D (m)**	**GDOP**	**PDOP**	**HDOP**	**VDOP**	**GPS SVs**
Open Field	1	0.0008	0.0004	0.0007	1.8 - 2.0	0.9 - 1.0	2.1 - 2.3	1.6 - 1.7	10/10
	2	0.0008	0.0004	0.0007	1.8	0.9	2.1	1.5 - 1.6	9/9
	3	0.0009	0.0005	0.0008	1.6 - 1.9	0.9 - 1.0	1.9 - 2.2	1.4 - 1.6	9/9
Tree	1	0.0046	0.0019	0.0042	2.5 - 3.6	1.1 - 1.2	2.9 - 4.3	2.2 - 3.3	8/9
	2	0.1346	0.0663	0.1171	2.2	1	2.5 - 2.6	1.9 - 2.0	8/8
	3	0.0027	0.0016	0.0022	1.4 - 2.1	0.8 - 1.3	1.6 - 2.4	1.2 - 1.6	9/10
Near Building	1	0.0046	0.0021	0.0041	7.5 - 8.9	3.3 - 3.9	9.6 - 11.4	6.7 - 8.0	5/7
	2	0.2827	0.1267	0.2527	9.7 - 10.4	4.5 - 4.8	12.6 - 13.4	8.6 - 9.2	5/5
	3	0.1231	0.0703	0.1010	2.0 - 3.6	1.3 - 2.2	2.3 - 4.4	1.5 - 2.8	7/7

Table 8: GNSS Solution Type and Number of Observations

Station	**Obs. #**	**Solution Type**	**GPS Observations**
Open	1	Phase Fixed	788/788
	2	Phase Fixed	684/684
	3	Phase Fixed	583/583
Tree	1	Phase Fixed	652/668
	2	Code	592/592
	3	Phase Fixed	584/650
Near Building	1	Phase Fixed	540/575
	2	Code	290/290
	3	Code	425/425

The following are diagrams representing the distribution of satellites observed for each station.

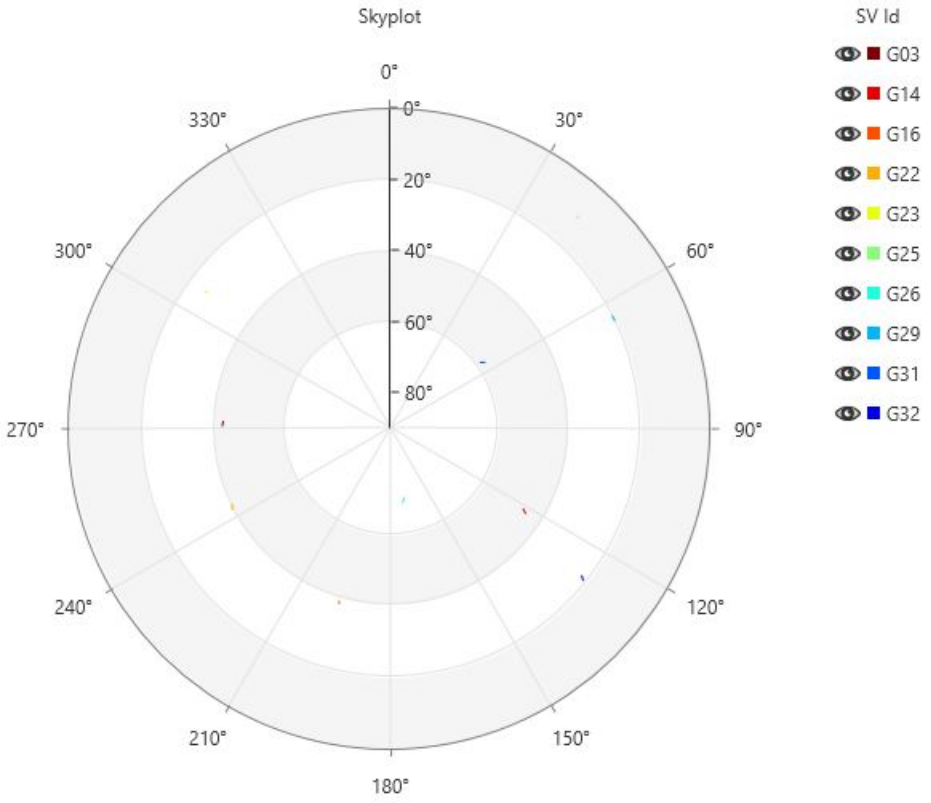

Figure 17: Satellite Distribution of 1st Observation of Open Field Point

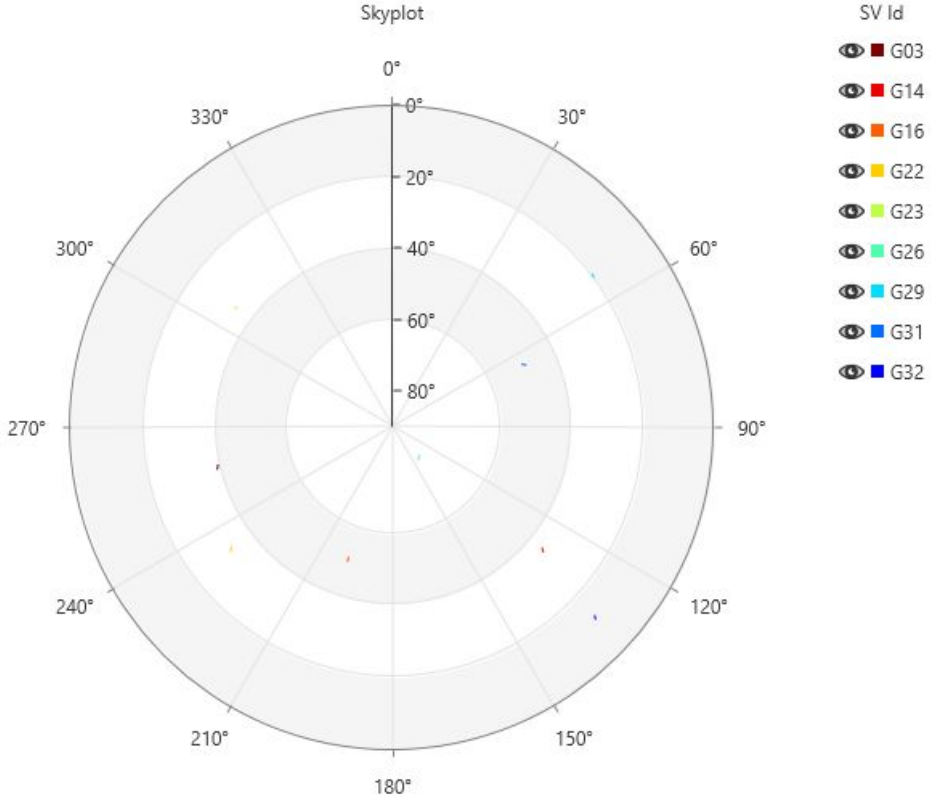

Figure 18: Satellite Distribution of 2nd Observation of Open Field Point

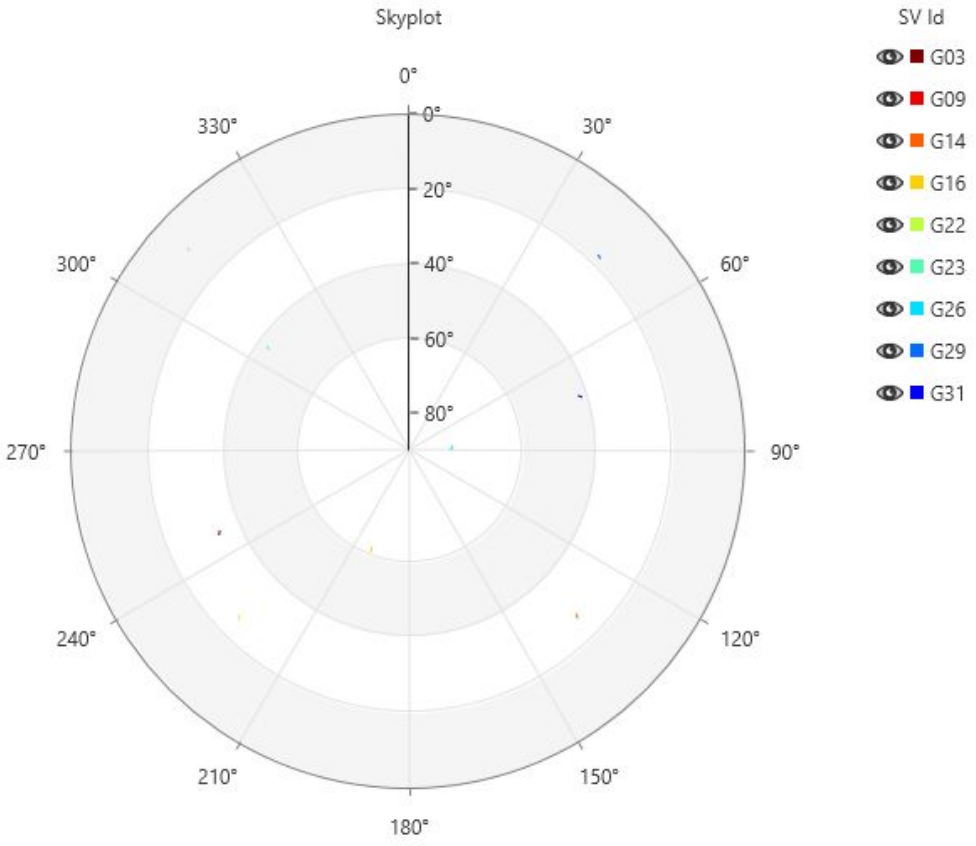

Figure 19: Satellite Distribution of 3rd Observation of Open Field Point

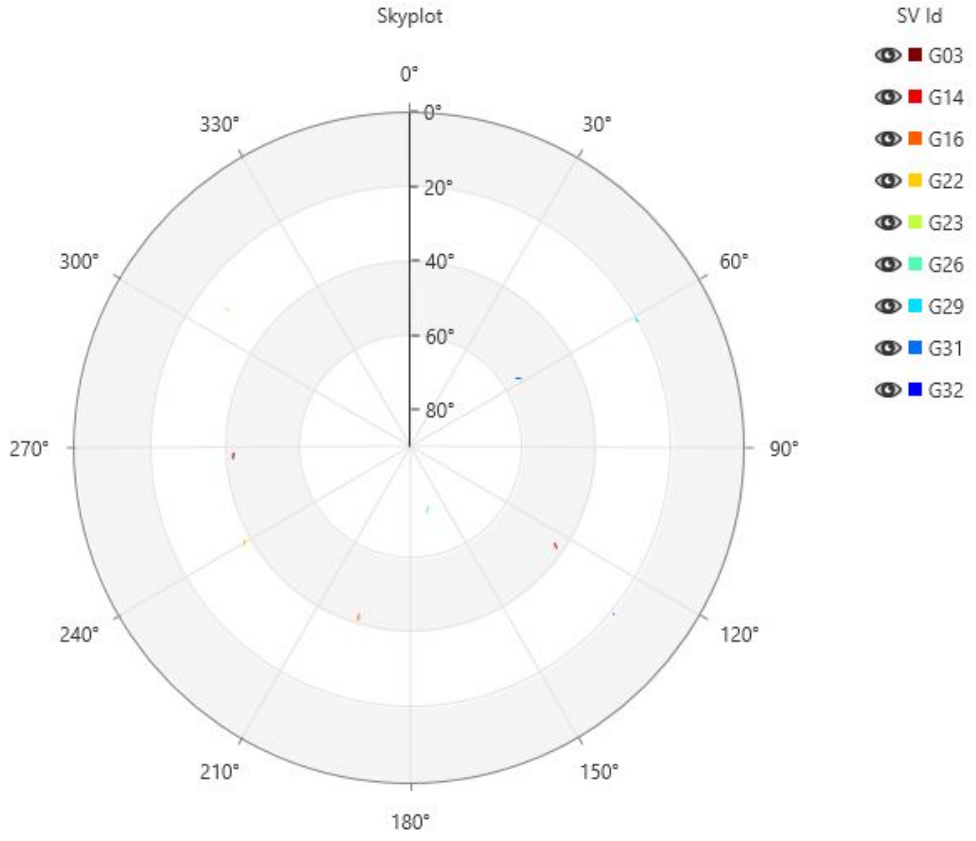

Figure 20: Satellite Distribution of 1st Observation of Under Tree Canopy Point

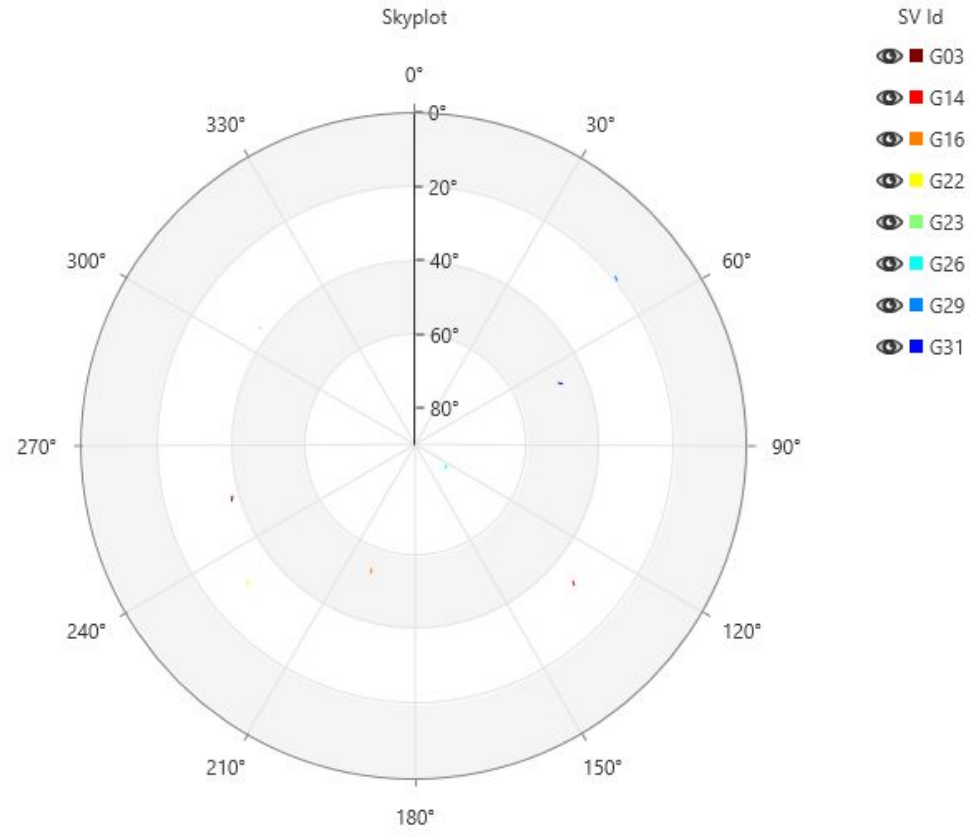

Figure 21: Satellite Distribution of 2nd Observation of Under Tree Canopy Point

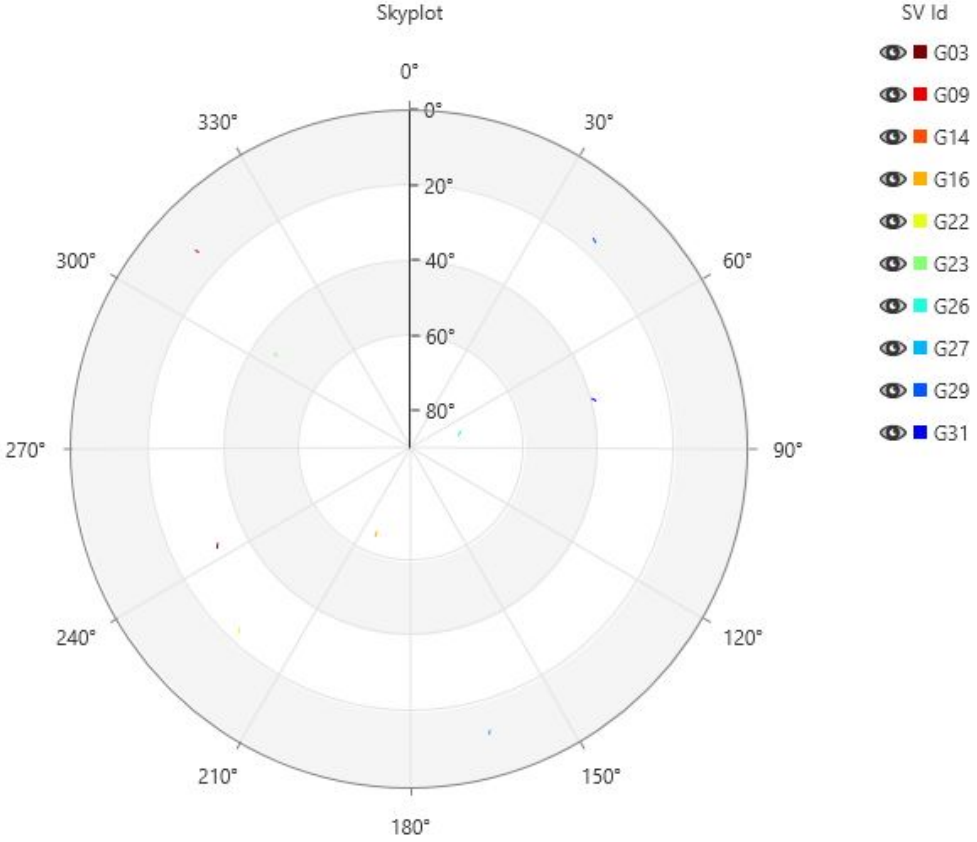

Figure 22: Satellite Distribution of 3rd Observation of Under Tree Canopy Point

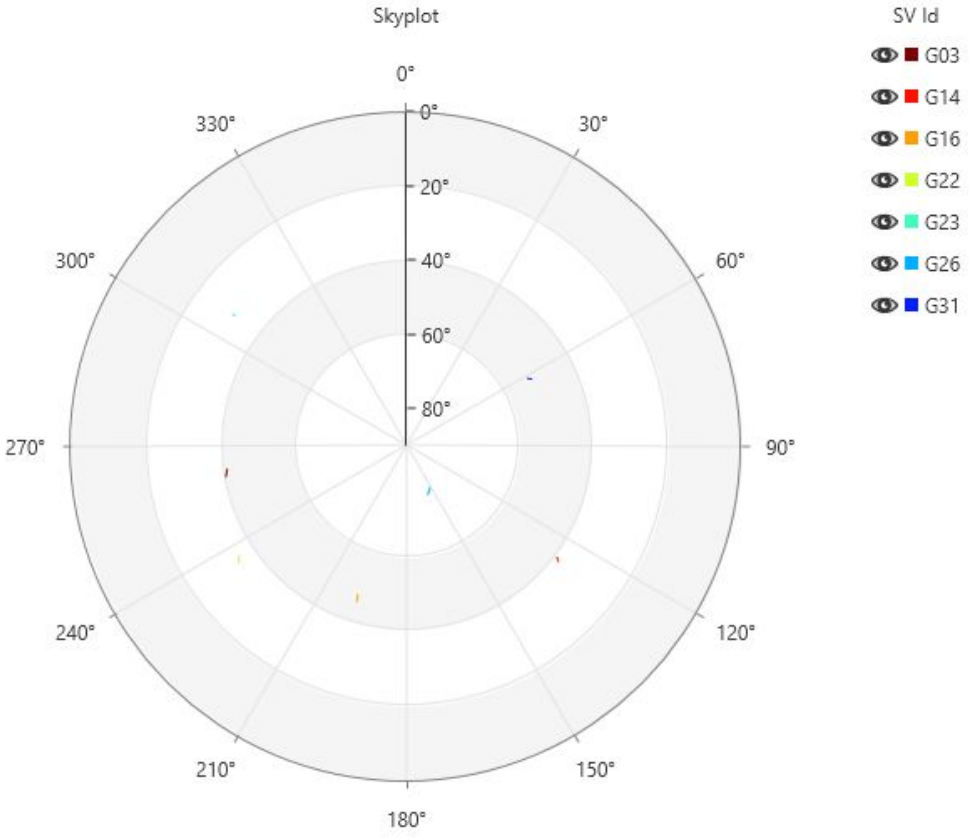

Figure 23: Satellite Distribution of 1st Observation of Near BuildingPoint

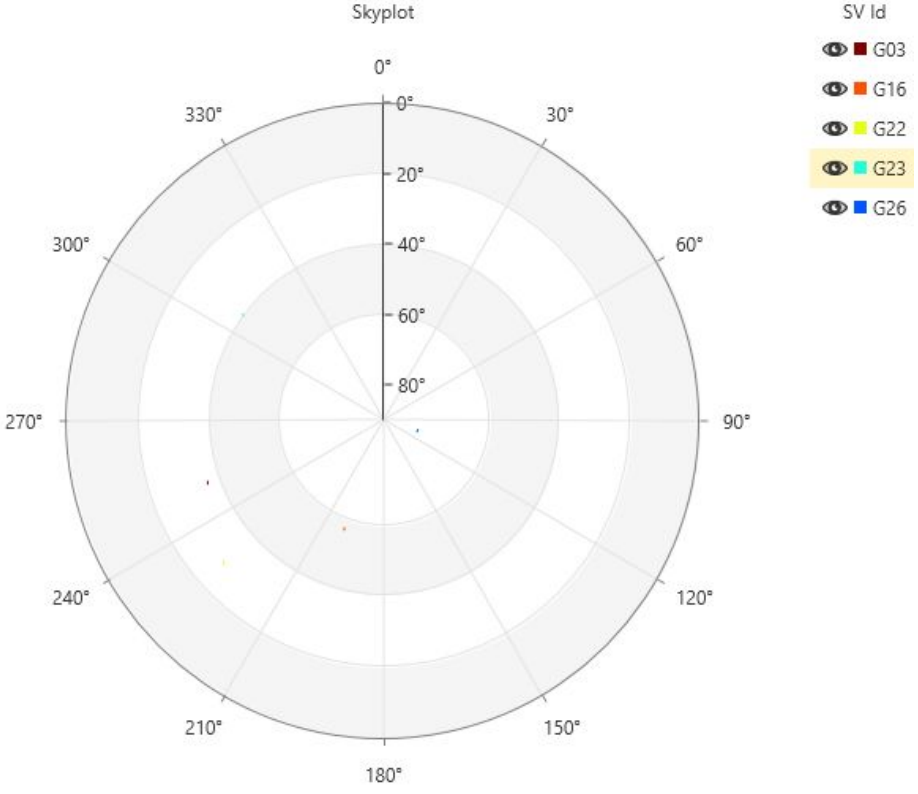

Figure 24: Satellite Distribution of 2nd Observation of Near BuildingPoint

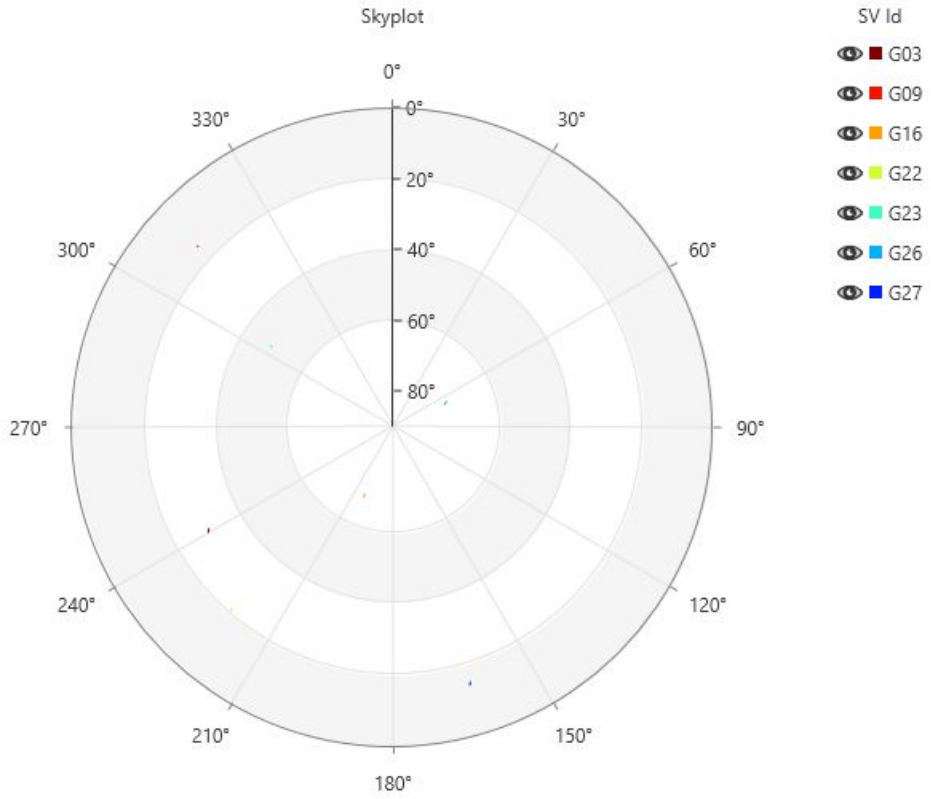

Figure 25: Satellite Distribution of 3rd Observation of Near BuildingPoint

Part 2: Static Data Processing and Analysis

The tables below summarize the results obtained by processing each of the seven baselines for under the scenarios listed above.

Table 9: Day 1 (November 25) Processed Baselines from *ALBH* Station to *BAMF Station*

Scenario	Baseline Components (m)			Slope Distance (m)	Standard Deviation (m)			
	ΔX	ΔY	ΔZ		σ_X	σ_Y	σ_Z	σ_{3D}
1	-79,388.3304	99,193.3971	32,741.5006	131,201.5354	0.0003	0.0003	0.0004	0.0006
4	-79,388.3359	99,193.4060	32,741.5116	131,201.5483	0.0005	0.0005	0.0007	0.0010
7	-79,388.3301	99,193.3975	32,741.4995	131,201.5352	0.0003	0.0003	0.0004	0.0006
8	-79,388.3296	99,193.3983	32,741.4977	131,201.5351	0.0003	0.0003	0.0004	0.0006
9	-79,388.3289	99,193.3992	32,741.4962	131,201.5350	0.0003	0.0004	0.0004	0.0006

Table 10: Day 2 (November 26) Processed Baselines from *ALBH* Station to *BAMF Station*

Scenario	Baseline Components (m)			Slope Distance (m)	Standard Deviation (m)			
	ΔX	ΔY	ΔZ		σ_X	σ_Y	σ_Z	σ_{3D}
1	-79,388.3198	99,193.4111	32,741.4762	131,201.5335	0.0003	0.0004	0.0005	0.0007
4	-79,388.3168	99,193.4219	32,741.4742	131,201.5393	0.0005	0.0006	0.0007	0.0010
7	-79,388.3193	99,193.4096	32,741.4760	131,201.5320	0.0003	0.0004	0.0005	0.0007
8	-79,388.3151	99,193.4219	32,741.4753	131,201.5386	0.0004	0.0005	0.0006	0.0008
9	-79,388.3107	99,193.4267	32,741.4714	131,201.5386	0.0004	0.0005	0.0006	0.0008

Table 11: Day 3 (November 27) Processed Baselines from *ALBH* Station to *BAMF Station*

Scenario	Baseline Components (m)			Slope Distance (m)	Standard Deviation (m)			
	ΔX	ΔY	ΔZ		σ_X	σ_Y	σ_Z	σ_{3D}

1	-79,388.3209	99,193.4016	32,741.4860	131,201.5295	0.0003	0.0004	0.0005	0.0007
4	-79,388.3247	99,193.4126	32,741.4818	131,201.5390	0.0004	0.0005	0.0007	0.0009
7	-79,388.3210	99,193.4020	32,741.4857	131,201.5297	0.0003	0.0004	0.0005	0.0007
8	-79,388.3151	99,193.4214	32,741.4692	131,201.5367	0.0004	0.0004	0.0005	0.0008
9	-79,388.3074	99,193.4246	32,741.4633	131,201.5330	0.0004	0.0004	0.0006	0.0008

Table 12: Day 4 (November 28) Processed Baselines from ALBH Station to *BAMF Station*

Scenario	Baseline Components (m)			Slope Distance (m)	Standard Deviation (m)			
	ΔX	ΔY	ΔZ		σ_X	σ_Y	σ_Z	σ_{3D}
1	-79,388.3256	99,193.3990	32,741.4926	131,201.5320	0.0003	0.0004	0.0004	0.0006
4	-79,388.3280	99,193.4158	32,741.4884	131,201.5451	0.0004	0.0005	0.0006	0.0009
7	-79,388.3256	99,193.3995	32,741.4920	131,201.5322	0.0003	0.0004	0.0005	0.0007
8	-79,388.3166	99,193.4241	32,741.4770	131,201.5416	0.0004	0.0004	0.0005	0.0008
9	-79,388.3084	99,193.4314	32,741.4681	131,201.5399	0.0004	0.0004	0.0006	0.0008

Table 13: Day 5 (November 29) Processed Baselines from ALBH Station to *BAMF Station*

Scenario	Baseline Components (m)			Slope Distance (m)	Standard Deviation (m)			
	ΔX	ΔY	ΔZ		σ_X	σ_Y	σ_Z	σ_{3D}
1	-79,388.3293	99,193.3943	32,741.4991	131,201.5322	0.0003	0.0003	0.0004	0.0006
4	-79,388.3328	99,193.4046	32,741.4945	131,201.5410	0.0004	0.0004	0.0005	0.0008
7	-79,388.3291	99,193.3946	32,741.4983	131,201.5322	0.0003	0.0003	0.0004	0.0006
8	-79,388.3201	99,193.4177	32,741.4796	131,201.5395	0.0003	0.0004	0.0005	0.0007
9	-79,388.3101	99,193.4230	32,741.4686	131,201.5348	0.0003	0.0004	0.0005	0.0008

Table 14: Day 6 (November 30) Processed Baselines from ALBH Station to *BAMF Station*

Scenario	Baseline Components (m)			Slope Distance (m)	Standard Deviation (m)			
	ΔX	ΔY	ΔZ		σ_X	σ_Y	σ_Z	σ_{3D}
1	-79,388.3175	99,193.4183	32,741.4707	131,201.5362	0.0004	0.0004	0.0006	0.0008
4	-79,388.3097	99,193.4356	32,741.4651	131,201.5432	0.0005	0.0005	0.0007	0.0010
7	-79,388.3173	99,193.4173	32,741.4701	131,201.5351	0.0004	0.0004	0.0005	0.0008
8	-79,388.2972	99,193.4443	32,741.4546	131,201.5395	0.0004	0.0004	0.0005	0.0008
9	-79,388.2882	99,193.4546	32,741.4461	131,201.5397	0.0004	0.0005	0.0006	0.0008

Table 15: Day 7 (December 1) Processed Baselines from ALBH Station to *BAMF Station*

Scenario	Baseline Components (m)			Slope Distance (m)	Standard Deviation (m)			
	ΔX	ΔY	ΔZ		σ_X	σ_Y	σ_Z	σ_{3D}
1	-79388.3248	99193.4034	32741.4860	131201.5332	0.0003	0.0004	0.0004	0.0006
4	-79,388.3337	99,193.4233	32,741.4819	131,201.5525	0.0004	0.0005	0.0006	0.0009
7	-79,388.3243	99,193.4044	32,741.4850	131,201.5333	0.0003	0.0003	0.0004	0.0006
8	-79,388.3249	99,193.4335	32,741.4690	131,201.5517	0.0003	0.0004	0.0005	0.0007
9	-79,388.3181	99,193.4390	32,741.4615	131,201.5499	0.0003	0.0004	0.0005	0.0008

Table 16: Average Slope Distance and its Standard Deviation Over Seven Days Under Each Scenario

	Scenario 1	Scenario 4	Scenario 7	Scenario 8	Scenario 9
Average Slope DIstance (m)	131201.5331	131201.5441	131201.5328	131201.5404	131201.5387
Standard Deviation (m)	0.0022	0.0050	0.0019	0.0054	0.0056

The meaning of the data in these tables will be discussed under the *Discussion Part 2* subheading below.

Discussion

Part 1: Static Data Collection and Processing

Inspecting the results for our observations, we see that the accuracy of the measurements is greatly influenced by the location of the station. That is, we see the largest uncertainty from stations close to buildings, followed by stations underneath tree canopies. The station that was out in the open enjoyed the greatest accuracy. In addition to this, we also see variations depending on the time that observations were carried out. These results are the product of multiple factors which contribute to system error.

To inspect the degree of uncertainty of our monitored points, one can inspect the cartesian standard deviations (STDs), or the 3D, 2D and 1D CQs. However, working in the cartesian coordinate system is not intuitive. As such, it is more beneficial to observe the CQs observed by the GNSS antenna. The 3D CQ reflects the total STD of a point in 3D spaces, while the 2D CQ reflects the total STD in the local horizontal. Thus, the 2D CQ describes the accuracy in the planar directions (North and East). Finally, the 1D CQ describes the STD in the vertical.

When comparing the 3D and 2D CQ, we see that open field station had consistently the smallest STD compared to the other stations, irrespective of observation number. This was expected as there were no obstructions due to canopies or structures for the signal being communicated from the satellites. As such, the station enjoyed full 360° (Azimuthal) visibility of available satellites. When inspecting the Skyplots for the open field station, we see that the antenna records signals from satellites surrounding it in all directions, including ones with low elevations (as low as ~ 15°), however, we do notice that there are no satellites between the azimuth range of 285° - 40°. In open environments, low elevations are able to become visible, when there are few obstructions surrounding the antenna. With no obstructions, the open field antenna was able to track and observe more satellites (seen in table 7), compared to the antenna at other stations.

When inspecting the dilution of precision (DOP) for the open field scenario, we see that it agrees with the results seen above. A lower DOP means that the satellites are better dispersed in the sky, and thus, we can determine the antenna's position with greater precision. As seen in the diagram below, a well dispersed satellite array results in a well defined point of intersection between multiple satellite pseudoranges. If the satellites are not spread out, then the pseudoranges overlap greatly, resulting in an ill defined point of intersection.

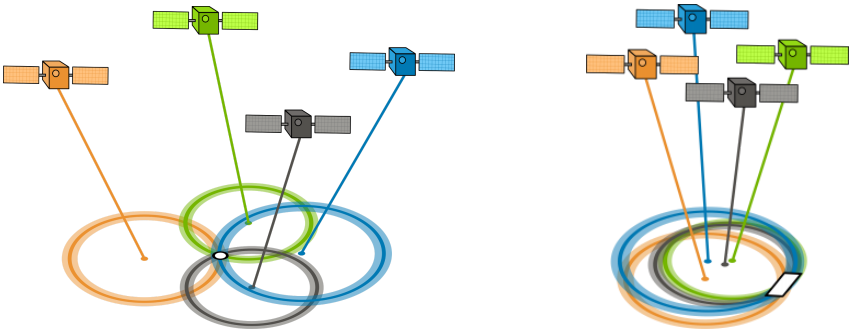

Figure 26: Satellite Dispersion and GDOP [gisgeography.com]

When inspecting the Horizontal Dilution of Precision (HDOP) and Vertical Dilution of Precision (VDOP) for the open field observations, we see that they are lower than the other station points. The one exception that stands out is that the 3rd tree observation shows a HDOP and VDOP range lower

than the open field scenario. Upon further inspection, we realize that this phenomenon stems from multiple observed satellites (from the tree canopy point) with an elevation of ~15° and an improved spread surrounding the antenna (full 360° azimuthal spread). Thus, it is reasonable for the HDOP and VDOP of the tree canopy point to be improved.

With better HDOP and VDOP, we see better Position Dilution of Precision (PDOP) and Geometric Dilution of Precision (GDOP). PDOP is a function of all 3D cartesian errors, while GDOP is a function of PDOP and the timing error.

$$PDOP = \sqrt{\sigma^2{}_x + \sigma^2{}_y + \sigma^2{}_z}$$
$$GDOP = \sqrt{PDOP^2 + \sigma^2{}_t}$$

In this manner, we see that the 4 DOP parameters are highly related to one another. With good DOP values, we see that the open field antenna enjoys accuracy to the sub-centimeter range.

When looking at the results for the antenna underneath the tree canopy, we see that the 3D and 2D CQ jumps to the centimeter range, in comparison to the open field position. Moreover, we see that the 2nd observation of the near tree point, experiences a large STD for the 3D and 2D CQ. Upon inspecting the DOPs and the Skyplot, we see that the variables are not significantly different or worse than the other near tree observations. However, inspecting the solution for our observation (seen in Table 8) we see that the second near tree observation is a code solution type, unlike the higher precision phase fixed solution type. In a code solution, the codes are matched up logically, however, this does not mean that they overlap perfectly. There is a bit of play between the GNSS signal and the Signal generated by the receiver. As such, the timing is not as accurate. For this reason, the second tree observation suffers more error than the other 2 instances.

Tree canopies are known to interfere with both the L1 and L2 GNSS signals. Although we were able to lock, research shows that a tree canopy decreases the signal to noise ratio, and increases cycle slips (Ogundipe, Ince & Bonenburg, 2016). As such, fewer observations are taken, a phenomenon that can be witnessed in our results. With fewer observations, the system is less redundant, and thus, the positional estimation is not as good.

Finally, inspecting the near building results, we see that the 3D and 2D CQ is in the tens of centimeter range, with the exception of the first observation set. This station's precision is considerably worse than that of the open field station. The first observation is comparable to that of the near tree station, however, this is due to the increased observation time that was allocated to the station (~4 minutes due to group blunder). When inspecting the number of GPS observations, we see that the first observation trial had substantially more observations than proceeding trials. As such, the accuracy of the measurement increases to levels seen in the near tree case. If not for the increased observation time, we would expect to see the accuracy drop. This argument is supported by the fact that the DOP for the 1st near building observation, is large, and thus, indicating that the satellite geometry is not ideal to support a high accuracy.

Finally, we also notice that the solutions of the near building point are all of code type. The exception to this trend was the first observation, which as discussed earlier enjoyed long observation length, allowing a phase fixed solution to be obtained.

Overall the near building station suffers from two main sources of error. The first source of error is the available geometry of satellites. Because a brick structure was to the East of the station, the antenna is limited in the satellites it can connect to the East of it (seen in the number of SVs tracked and observed). When looking at the Skyplots, we see this to be true, as no Eastern satellites were connected with a low elevation. There was one satellite to the East that was observed, however, this satellite had a high elevation, and this was almost above the point of interest. As such, visibility existed between this satellite and our antenna at the near building station.

The other source of error for our near building station was multipath error. This error stems from a satellite signal bouncing off of structures, prolonging travel time, and thus, providing

erroneous pseudoranges. This phenomenon is frequently observed in urban landscapes, where tall structures exist surrounding a GNSS antenna. To no surprise, the wall of the neighbouring structure to our near building point, exposed our observation to multipath error. As such, this station sees the greatest error in comparison to other points.

When inspecting the accuracy of each observation along the vertical (1D CQ), we see similar trends to that of the 3D and 2D CQ. In general, the open field station enjoys the greatest accuracy followed by the near tree station, and then followed by the near building point. In general, we see that the error in the vertical is greater than the error in the horizontal direction. This is expected as the geometry of signals does not support strong accuracies in the vertical. In order to obtain an accurate vertical measurement, our antenna would need to be able to detect signals on the other side of the planet (underneath the antenna), however this is simply not feasible.

Inspecting the Skyplots, we see that the geometry of the satellites changes through time. This was expected, however, the influence on our observations was not as clear. We see that between trials we roughly had the same number of satellites, with the exceptions of a few scenarios. Similarly, the DOP was roughly the same for all trials of the same station. Those that exhibited large changes in DOP were also influenced by other factors such obstructions, which limited satellite visibility and thus, influenced the DOP.

Part 2: Static Data Processing and Analysis

Recalling for this section, static observations over a period of seven days for two different base stations in Victoria, British Columbia were downloaded and analyzed. The parameters for these observations were adjusted to test how frequency and elevation cutoff affected the quality of the observations. The intent was to also analyze the effect the data arc in hours would affect the quality as well, but the Leica Affinity software did not allow this option. Therefore, there are five different scenarios that will be compared. The characteristics of the five scenarios are shown in the table below:

Table 17: Scenarios for Part 2 Data Processing and Analysis

Scenario #	Data arc (hours)	Frequencies	Elevation cutoff (°)
1	24	L1 and L2	10
2	12	L1 and L2	10
3	1	L1 and L2	10
4	24	L1	10
5	12	L1	10
6	1	L1	10
7	24	L1 and L2	15
8	24	L1 and L2	20
9	24	L1 and L2	25

Effect of Frequency on Results

In general, we observed that using two frequencies instead of one increased the quality of the results, and increasing the elevation cutoff decreased the quality of the results. The following graphs and charts will be used to discuss this further. As seen through tables 9-15, three main types of information were recorded for each scenario: the changes in coordinates of rover station from the reference station, the slope distance between the rover and reference station, and the standard deviations of the changes.

First, we consider the effect of the number/type of frequencies used in processing. In particular, Scenario 1 and 4 were compared. Scenario 1 made us of the L1 and L2 frequencies while Scenario 4 only used the L1 frequency.

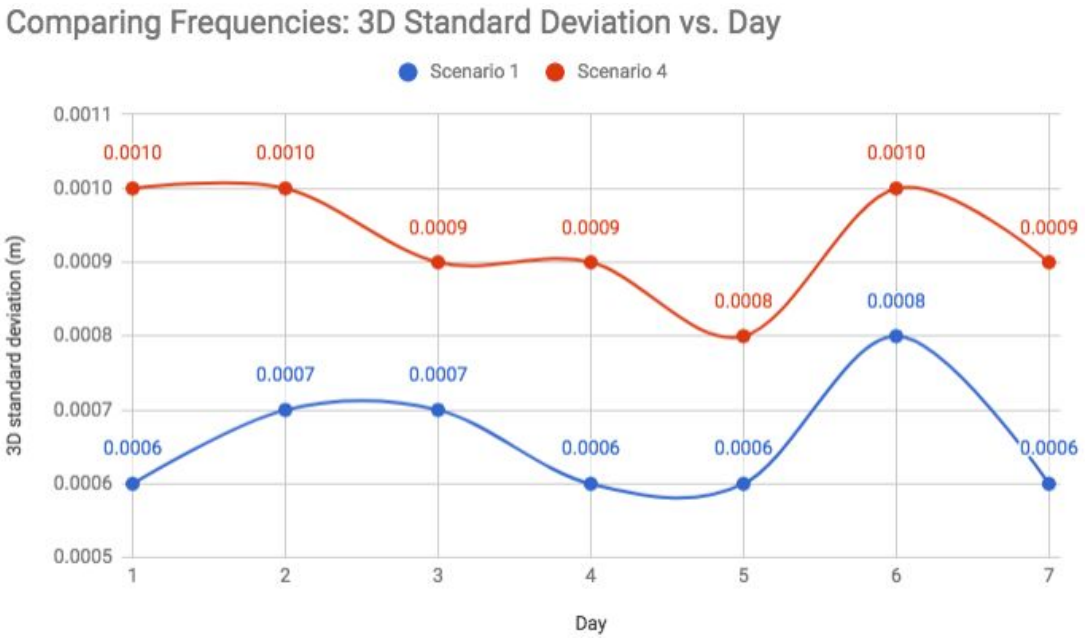

Figure 27: Effect of Frequency on Error Results

Figure 27 above shows the 3D standard deviations for each day for Scenario 1 and 2. The 3D standard deviations are calculated using the standard deviation of the X, Y and Z components. The figure shows that using one frequency (Scenario 4) consistently resulted in a higher standard deviation than using two frequencies (Scenario 1). This is reinforced by the fact that the average 3D standard deviation over the seven days was 0.93mm for one frequency (Scenario 4) and 0.66mm for two frequencies (Scenario 1); a difference of 0.27mm.

Figure 28 below shows the slope distance of the baseline between the two base stations for each day observed. This graph can be used to analyze the consistency of the two scenarios. Scenario 1 has an average slope distance of 131201.5331m while Scenario 2 has an average slope distance of 131201.5441m which is a difference of 0.011m (see Table 16). However, the slope distances for Scenario 2 are spread out more and this is reflected by the standard deviation of the slope distance over the seven days. For Scenario 1, the standard deviation is 0.0022m while for Scenario 4 it is 0.0050m (see Table 16). This means that Scenario 1 (which made use of two frequencies) gets more consistent results.

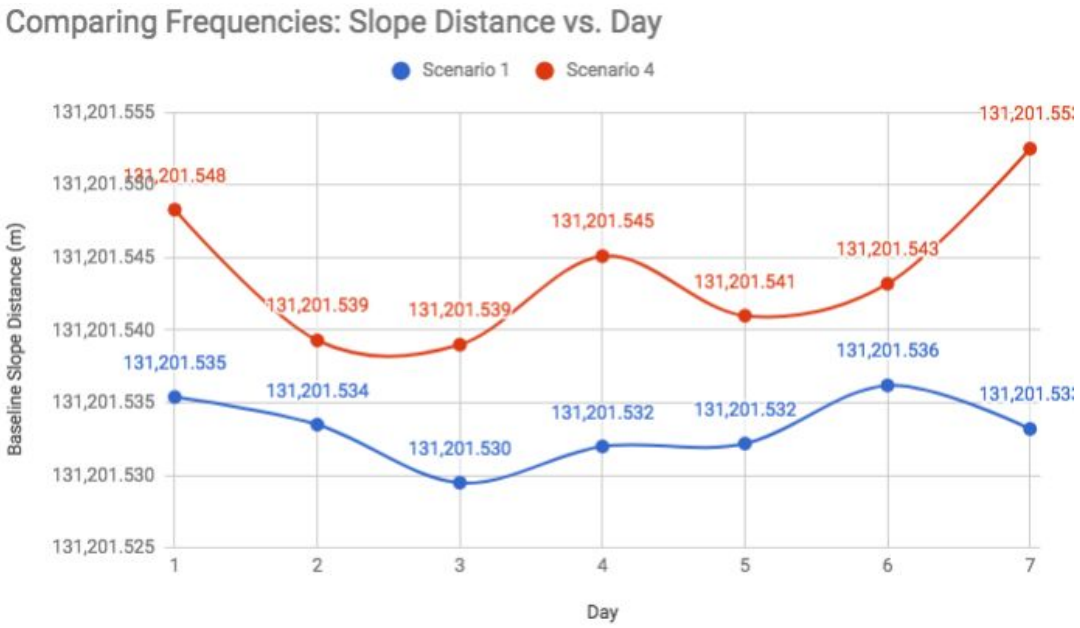

Figure 28: Effect of Frequency on Slope Distance Results

Figure 29 below further reinforces the notion that processing results are more consistent when using two frequencies instead of one. Figure 29 shows the location of the X&Y Cartesian coordinates for each day observed for Scenario 1 and 4. The scenario and day for each point is referred to by a label: for example, “S1 D1” refers to Scenario 1, Day 1. Each section of the grid is 5mm by 5mm. It is easily evident from this graph is that the observations for Scenario 4 are spread out more than for Scenario 1. The results for Scenario 4 are spread out over an area roughly 3.5cm by 3cm while the results for Scenario 1 are spread out over an area of roughly 3cm by 1.5cm. Figure 29 also shows the average position for each scenario over the seven days. These average positions might be a better indicator of the true position of the base station as they are the average of a week’s worth of observations. For example, for both Scenario 1 and 4, day 6 produced results that are much farther northeast than the rest of the results. Using the average over the week allows these outliers to be discounted.

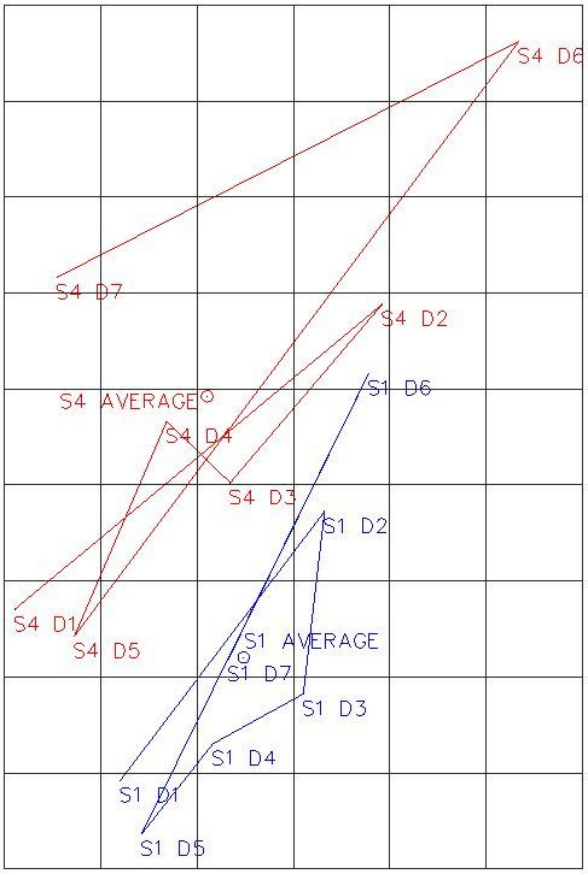

Figure 29

In conclusion, the data collected show that using two frequencies instead of one frequency led to increased quality of observations. This is likely because using two frequency sources instead of one frequency source increases the quality of the observations because it adds more redundant data to the calculation of the position. In addition, by considering two frequencies (L1 and L2), the ionospheric delay error of the satellite can be directly measured and removed, otherwise it must be accounted for using a generic model or outside source - making it more likely to be less accurate (GeoConnect, n.d.). Thus, it is reasonable to observe greater error in the data processing results (or larger standard deviation values)

Effect of Elevation Cut-off Angle on Results

The elevation cut-off angle it the angle above the horizon used to determine which satellite signals to use for ranging. For example, when the elevation cutoff angle is set at 10 degrees, the receiver will only use signals from satellites that are more than 10 degrees above the horizon in its calculation of position. Recalling, scenario 1 used an elevation cutoff angle of 10 degrees, Scenario 7 used 15 degrees, Scenario 8 used 20 degrees, and Scenario 9 used 25 degrees.

Figure 30 below shows the 3D standard deviation for each day for each scenario. This graph shows that the two scenarios with a lower cutoff angle (10 and 15 degrees) also have a lower 3D standard deviation that the cut off angles of 20 and 25 degrees. Scenarios 8 and 9 with higher cutoff angles (20 and 25 degrees respectively) have higher 3D standard deviations. The average of the 3D standard deviations over the seven days reinforce this trend. The 3D standards deviations for Scenario 1, 7, 8 and 9 were 0.66mm, 0.67mm, 0.74mm, and 0.77mm, respectively. Thus, we hypothesize that a smaller cut-off angle, increases the accuracy of the processed results.

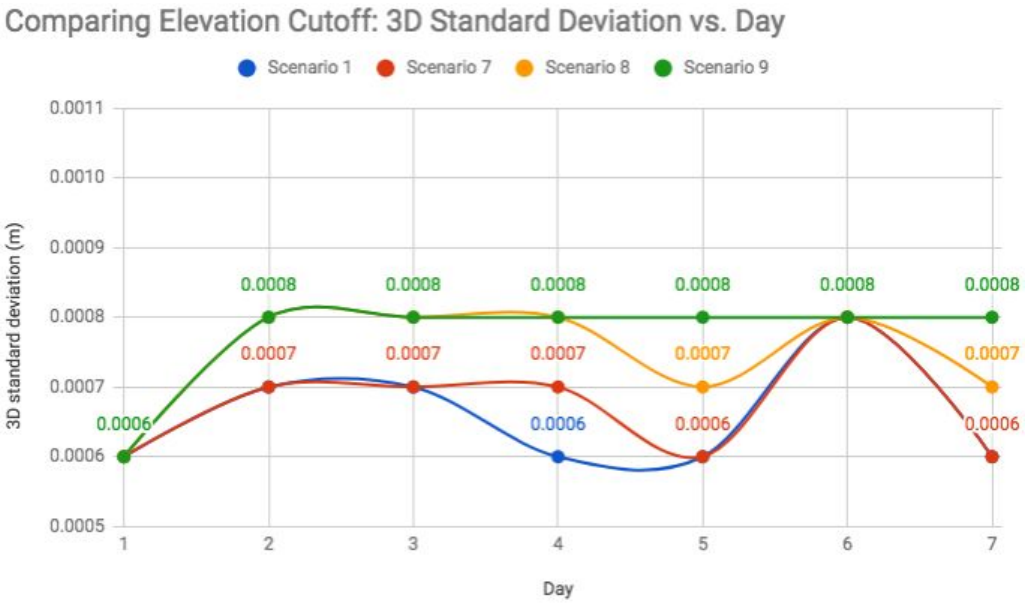

Figure 30: Effect of Cut-Off Angle on Error Results

Figure 31 below shows the slope distance of the baseline between base stations for each of the seven days of observations. This graph shows that using a cutoff angle of 10 and 15 degrees resulted in a very similar distance that was quite consistent over the seven days. This is illustrated by the average positions for Scenario 1 and 7 of 131,201.5331m and 131,201.5328m which were 0.3mm apart from each other (Table 16). Furthermore, the standard deviation of the slope distance over the seven days was 2.2mm and 1.9mm (Table 16). However, the baseline distance calculated using a cutoff angle of 20 and 25 degrees were not as close as they were to the results for determined for Scenario 1 and 7 nor were they as consistent. The average slope distance over the seven days for Scenarios 8 and 9 were 131,201.5404m and 131201.5387mm respectively with standard deviations of 5.4mm and 5.6mm respectively (Table 16). Therefore, using lower cutoff angles led to more consistent results.

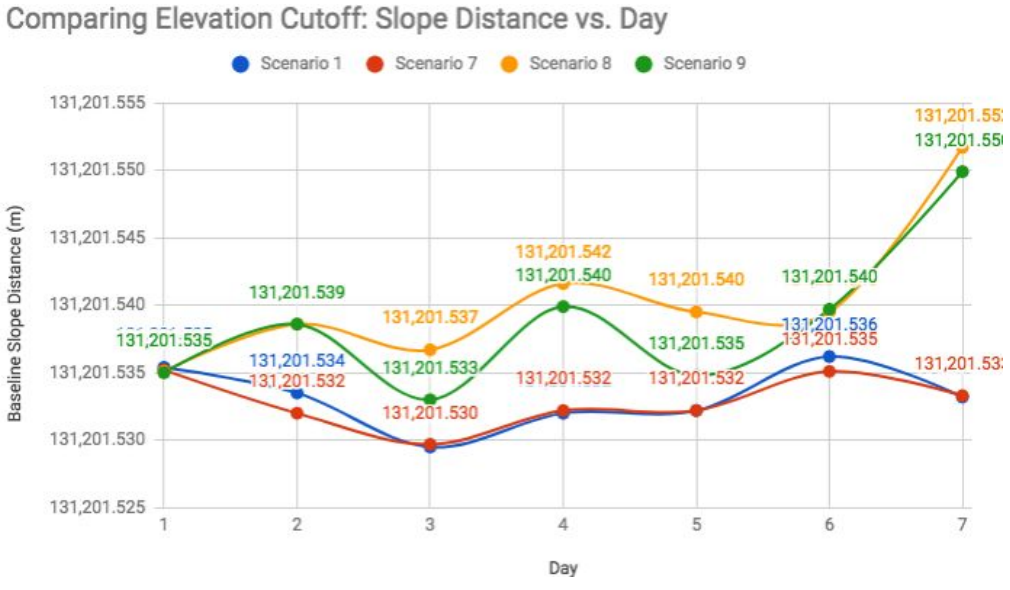

Figure 31: Effect of Cut-Off Angle on Slope Distance Results

Finally, Figure 32 is similar to Figure 29 above as it shows the location of the X & Y Cartesian coordinates for each day for the four scenarios. This figure reinforces that the position

determined increases as the elevation angle increases. Again, Scenarios 1 and 7 are very similar and over the seven days are spread out over an area roughly 3cm by 1.5cm whereas Scenario 8 is over an area roughly 5.5cm by 3.5 cm, and Scenario 9 is over an area roughly 6.5cm by 4.5cm. The position for the average coordinate values for each scenario are also shown which shows that as the cutoff angle increases, the position drifts to the northeast.

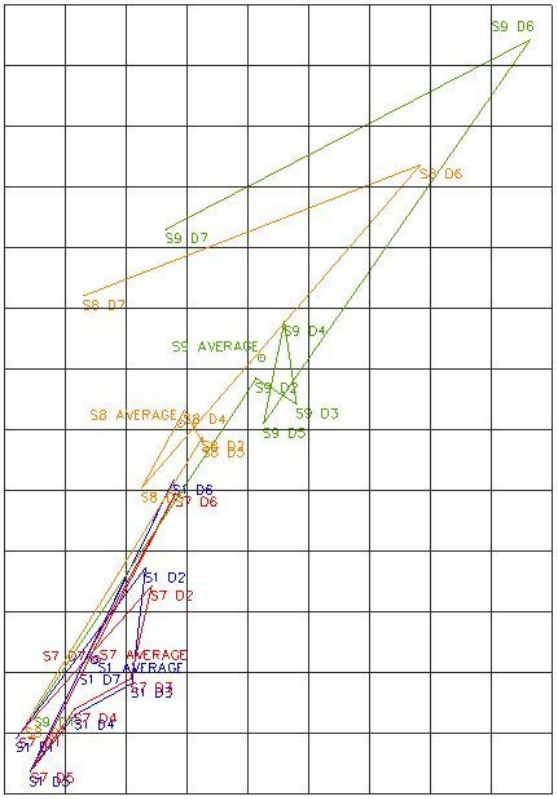

Figure 32

The reduced quality of the results as the cutoff angle increases is likely because of two reasons. First, a higher cutoff angle means not as many satellites are used to calculate the solution, as fewer signals are detected or used. Fewer satellites and their signals results in less redundant data. Second, increasing the cutoff angle means that the geometry used for the ranging isn't as good. When ranging, having a greater satellite spread from the point other allows for a better calculation of the points position, as there is less likelihood for bias. Increasing the cut off angle means that the satellites used for calculating position are not spread out as much; therefore the quality decreases.

Conclusion

In end, further practice with working with GPS signals and GPS data processing was acquired. It was found that the station set up/location greatly influenced the accuracy of measurements. If located close to a building and under tree canopies, the station results showed greater uncertainty. This was a result of the dilution of precision and multipath of the received signals. Furthermore, it was found that using a greater number of frequencies to process the data, mainly L1 and L2 frequencies, and lower cut-off angles resulted in more consistent results that had a lower magnitude of error.

Work Breakdown

Team Member	Contribution
Agata Szeremeta	- Processed data for task 2 - Wrote up procedures for office portion of task 2 - Composed milestone write ups - Collated report and powerpoint - Helped develop powerpoint
Dawid Szeremeta	- Processed data for task 1 - Wrote up procedures for office portion of task 1 - Discussed results for task 1 - Helped develop powerpoint
Colin Vanderwoerd	- Discussed results for task 2 - Generated plots for task 2 - Helped develop powerpoint
Mitch Palmer	- Wrote executive summary - Wrote Introduction - Wrote up part 1 field procedures

References

British Columbia. (n.d.). *The MapPlace - BC Map UTM Projection*. Retrieved 02 05, 2018, from Ministry of Energy, Mines, and Petroleum Resources: http://www.empr.gov.bc.ca/MINING/GEOSCIENCE/MAPPLACE/MAINMAPS/Pages/BCUTMZones.aspx

GeoConnect. (n.d.). *GSP Signals (L1, L2, L5)*. Retrieved 02 11, 2018, from GeoConnect: http://geoconnect.com.au/gps-signals-l1-l2-l5/

Ogundipe O., Ince S., & Bonenburg L. (January 2016). GNSS Positioning Under Forest Canopy. Conference Paper. Retrieved on February 10, 2018 from: researchgate.net/publication/262484519_GNSS_Positioning_Under_Forest_Canopy

Appendix A: Post Processing Results for Part 1

Point Id	Solution Type	Frequ...	Easting [m]	Northing [m]	WGS84 Latitude [°]	WGS84 Longitude [°]
building1	Phase Fixed	L1/L2	619,879.3897	4,847,894.1498	43° 46' 27.82" N	79° 30' 37.45" W
⚠ building2	Code	L1/L2	619,880.0414	4,847,895.0755	43° 46' 27.85" N	79° 30' 37.42" W
⚠ building3	Code	L1/L2	619,879.4688	4,847,893.9523	43° 46' 27.82" N	79° 30' 37.44" W
open1	Phase Fixed	L1/L2	619,830.8630	4,847,913.7597	43° 46' 28.49" N	79° 30' 39.60" W
open2	Phase Fixed	L1/L2	619,830.8582	4,847,913.7668	43° 46' 28.49" N	79° 30' 39.60" W
open3	Phase Fixed	L1/L2	619,830.8617	4,847,913.7648	43° 46' 28.49" N	79° 30' 39.60" W
tree1	Phase Fixed	L1/L2	619,857.8674	4,847,921.6605	43° 46' 28.73" N	79° 30' 38.39" W
⚠ tree2	Code	L1/L2	619,857.9682	4,847,922.1434	43° 46' 28.74" N	79° 30' 38.38" W
tree3	Phase Fixed	L1/L2	619,857.8840	4,847,921.6592	43° 46' 28.73" N	79° 30' 38.39" W

Figure : Local and WGS84 Geodetic Coordinates for Station Points

Point Id	WGS84 Ellip...	WGS84 Cartesian X [m]	WGS84 Cartesian Y [m]	WGS84 Cartesian Z [m]	Δx [m]	Δy [m]	Δz [m]
building1	158.5376	839,823.2107	-4,535,876.2056	4,390,135.4156	39.6910	-90.8487	-104.8546
⚠ building2	157.4473	839,823.6095	-4,535,874.6879	4,390,135.3213	40.0898	-89.3310	-104.9489
⚠ building3	158.2231	839,823.2687	-4,535,876.1038	4,390,135.0544	39.7490	-90.7469	-105.2158
open1	155.8728	839,772.9074	-4,535,869.1496	4,390,148.3632	-10.6123	-83.7927	-91.9070
open2	155.9089	839,772.9066	-4,535,869.1713	4,390,148.3934	-10.6131	-83.8144	-91.8768
open3	155.9496	839,772.9156	-4,535,869.2010	4,390,148.4201	-10.6041	-83.8440	-91.8501
tree1	156.8638	839,798.7988	-4,535,859.8661	4,390,154.4035	15.2791	-74.5092	-85.8667
⚠ tree2	157.1381	839,798.8820	-4,535,859.7137	4,390,154.9407	15.3623	-74.3568	-85.3295
tree3	156.9257	839,798.8234	-4,535,859.9082	4,390,154.4452	15.3038	-74.5512	-85.8250

Figure : Cartesian Coordinates and Baseline Components for Station Points

Point Id	Slope Dist. [m]	SD Δx [m]	SD Δy [m]	SD Δz [m]	CQ 3D [m]	CQ 2D [m]	CQ 1D [m]	GDOP	PDOP	HDOP	VDOP
building1	144.3030	0.0014	0.0034	0.0029	0.0046	0.0021	0.0041	9.6 - 11.4	7.5 - 8.9	3.3 - 3.9	6.7 - 8.0
⚠ building2	143.5322	0.0869	0.2101	0.1680	0.2827	0.1267	0.2527	12.6 - 13.4	9.7 - 10.4	4.5 - 4.8	8.6 - 9.2
⚠ building3	144.5177	0.0469	0.0899	0.0696	0.1231	0.0703	0.1010	2.3 - 4.4	2.0 - 3.6	1.3 - 2.2	1.5 - 2.8
open1	124.8228	0.0002	0.0005	0.0006	0.0008	0.0004	0.0007	2.1 - 2.3	1.8 - 2.0	0.9 - 1.0	1.6 - 1.7
open2	124.8152	0.0002	0.0005	0.0006	0.0008	0.0004	0.0007	2.1	1.8	0.9	1.5 - 1.6
open3	124.8147	0.0003	0.0006	0.0006	0.0009	0.0005	0.0008	1.9 - 2.2	1.6 - 1.9	0.9 - 1.0	1.4 - 1.6
tree1	114.7091	0.0011	0.0030	0.0033	0.0046	0.0019	0.0042	2.9 - 4.3	2.5 - 3.6	1.1 - 1.2	2.2 - 3.3
⚠ tree2	114.2194	0.0395	0.0867	0.0950	0.1346	0.0663	0.1171	2.5 - 2.6	2.2	1.0	1.9 - 2.0
tree3	114.7085	0.0009	0.0018	0.0018	0.0027	0.0016	0.0022	1.6 - 2.4	1.4 - 2.1	0.8 - 1.3	1.2 - 1.6

Figure : Slope Distance, Baseline Standard Deviations and DOPs for Station Points

	Point Id	Cut-Off...	Tropospheric Model	Ionospheric Model	GPS SVs	GPS Obs	Common Epochs	Fixed Epochs [%]
	building1	11.1111	VMF with GPT2 model	Computed	5/7	540/575	54	100
⚠	building2	11.1111	VMF with GPT2 model	Computed	5/5	290/290	29	-
⚠	building3	11.1111	VMF with GPT2 model	Computed	7/7	425/425	32	-
	open1	11.1111	VMF with GPT2 model	Computed	10/10	788/788	42	100
	open2	11.1111	VMF with GPT2 model	Computed	9/9	684/684	38	100
	open3	11.1111	VMF with GPT2 model	Computed	9/9	583/583	35	100
	tree1	11.1111	VMF with GPT2 model	Computed	8/9	652/668	42	100
⚠	tree2	11.1111	VMF with GPT2 model	Computed	8/8	592/592	37	-
	tree3	11.1111	VMF with GPT2 model	Computed	9/10	584/650	38	100

Figure : Number of GPS SV connected to Along with Additional Properties